Structural evolution within the one-phase region of a three-component microemulsion system: Water–n-decane–sodium-bis-ethylhexylsulfosuccinate (AOT)

S.-H. Chen, S.-L. Chang, and R. Strey

Citation: The Journal of Chemical Physics **93**, 1907 (1990); doi: 10.1063/1.459068
View online: http://dx.doi.org/10.1063/1.459068
View Table of Contents: http://scitation.aip.org/content/aip/journal/jcp/93/3?ver=pdfcov
Published by the AIP Publishing

Structural evolution within the one-phase region of a three-component microemulsion system: Water–*n*-decane–sodium-bis-ethylhexylsulfosuccinate (AOT)

S.-H. Chen and S.-L. Chang
Nuclear Engineering Department, 24-211 Massachusetts Institute of Technology, Cambridge, Massachusetts 02139

R. Strey
Max-Planck-Institut fur Biophysikalische Chemie Postfach 2841, D-3400 Gottingen, FRG

(Received 29 June 1989; accepted 30 April 1990)

The continuous inversion from a water-in-oil (w/o) microemulsion at low temperatures to an oil-in-water (o/w) microemulsion at higher temperatures within the one-phase channel of water (0.6% NaCl)–*n*-decane–AOT microemulsion system is investigated by small angle neutron scattering (SANS). At constant AOT (surfactant) weight fraction γ of 12%, the structural evolution as a function of temperature takes place in different forms as the oil-to-water weight fraction α is varied from 15 to 90 %. At low o-w weight fractions ($\alpha = 15$ and 20 %) the microemulsions transform from a water-internal, oil-continuous structure at lower temperatures to an oil-internal, water-continuous droplet structure at higher temperatures jumping across an intermediate region of a lamellar phase (L_α). However, at higher o-w weight fractions ($\alpha = 80$ and 90 %) the evolution goes through a stage of percolation of the water droplets first into extended water clusters, then the structural inversion takes place probably through a transition of these water clusters into an entangled tubular structure. At equal oil-to-water volume ration ($\alpha = 40\%$), the structure can be described as bicontinuous at both low and high temperatures. In this case we are able to extract two lengths characterizing the structure from SANS data using different models for the scattering length density fluctuation correlation function of a bicontinuous microemulsion.

I. INTRODUCTION

Three-component microemulsions are thermodynamically stable, isotropic liquid mixtures characterized by simultaneous solubilization of large amounts of two immiscible liquids, water and oil, by comparatively small amounts of amphiphiles. Experience shows that an amphiphilic molecule displays its highest solubilization efficiency when it is equally well soluble in oil and water, that is when it is balanced with respect to its preference to the oil and water. An anionic surfactant AOT (sodium-bis-ethylhexylsulfosuccinate) is almost balanced with respect to water and commonly used oils at ambient temperature.[1] By virtue of this feature it has become the most widely studied amphiphile for the purpose of formulating microemulsions. One significant virtue of AOT is that it does not require a cosurfactant to form microemulsions, a feature which considerably simplifies the presentation of the phase behavior of the microemulsions and the interpretation of experimental data.

This paper is the first in a series of papers studying the details of the microstructure of microemulsions made from water (0.6% NaCL)–*n*-decane–AOT. The system has been selected for two basic reasons: First, there exists a large body of experimental data for the water–oil–AOT system. These include SANS,[2–5] electrical conductivity,[6–9] field jump,[9,10] NMR self diffusion,[11,12] interfacial properties,[13,14] dynamics,[15] and reaction kinetics,[16–18] just to mention only the recent publications. Second, addition of small amounts of an inert electrolyte, such as NaCl, has a large effect on the phase behavior of the microemulsions. In general, an ionic amphiphile, and in particular AOT, can be made to change from lipophilic to hydrophilic by raising the solution temperature. This is because on increasing temperature, the effective fractional dissociation of the counterion will increase. On the other hand, addition of NaCl has an exactly opposite effect. It will make AOT less hydrophilic, because the salt ions will compete with the counterions and the head groups for water of hydration. This combination of addition of NaCl and raising the temperature can be used to tune the phase behavior of water (NaCl)–*n*-decane–AOT microemulsion systems with precision. For example, an addition of 0.6% NaCl to water allows an observation in this system of the general pattern of the phase behavior of a water–oil–ionic amphiphile microemulsion system.[19,20] A particularly important feature is the appearance of a three-phase body in the phase prism at a convenient temperature range (40 ± 15 °C). In the vicinity of this three-phase body, one finds an adjacent one-phase region where the highest mutual solubility of water and oil and the lowest interfacial tension between the aqueous and the oleic phase are realized. Both these properties are of great interest to industry and research. For microemulsion systems formulated from nonionic surfactants, a recently published compilation of a variety of experimental results[21] has demonstrated the diversity of properties ranging from ultralow interfacial tensions and wetting phenomena, to percolation transition from disconnected to bicontinuous structure for the microstructure of microemulsions in the one-phase region. A notable feature for the phase behavior of nonionic microemulsions is that the role of temperature is

 0021-9606/90/151907-12$03.00

exactly opposite to that in ionic microemulsions. The reason for that is, on raising the temperature, there will be less hydrogen bonds formed between the head groups and water. This will render the amphiphile less hydrophilic.

From the point of view of conducting scattering experiments for investigation of the microstructure, microemulsions in the one-phase region offer a number of advantages as compared to the traditionally emphasized middle phase of the three-phase microemulsions.[22-24] In a one-phase microemulsion, composition of water, oil, and amphiphile is completely fixed by the preparation of the sample and is invariant to temperature variation. This is a very convenient feature for carrying out a SANS measurement because one does not have to worry about the temperature variation and its associated composition variation (as for the case of the middle phase microemulsion) often happen during the transfer of sample from the container to the SANS spectrometer. Furthermore, for microemulsions in the one-phase region one has a complete freedom in choosing the surfactant weight fraction γ and the relative oil-to-water weight fraction α. This flexibility allows investigation of the evolution of the microstructure as a function of temperature at a given set of γ and α. Last, but not the least, the one-phase region is bounded on the top and the bottom (in temperature) by two-phase microemulsions, which are respectively the o/w and w/o types. Thus the inversion of the microstructure across the one-phase channel is expected on an intuitive ground. A large number of SANS investigations of the microstructure of one-phase microemulsions in AOT based systems in the past concluded invariably that the microemulsions consisted of polydispersed water droplets dispersed in oil.[2-5] Since without addition of salt, one cannot realize a three-phase body at the experimentally accessible temperature range, these one-phase microemulsions are likely to be of the droplet type, away from the three-phase body. In this series of experiments we are able to circumvent this restriction.

After a brief experimental section, II, we describe the general phase behavior of a water–oil–amphiphile system with an application to D_2O (NaCl)–*n*-decane–AOT system in Sec. III. From the detailed knowledge of the phase behavior, well-defined paths in the phase diagram were selected for the SANS study of the microstructure. In particular we shall present results obtained in the one-phase region, adjacent to the three-phase body, at a constant surfactant concentration $\gamma = 12\%$, varying the oil-to-water ratio α and temperature T. Section IV describes the analyses of the scattering data according to different regions of α. Section V discusses the microstructures inferred from these analyses. Section VI gives a brief summary and the prospect.

II. EXPERIMENTAL

Materials. The amphiphile AOT (sodium-bis-ethylhexylsulphosuccinate) was obtained from Fluka and purified according to the procedure developed by Kunieda and Shinoda.[1] The purified product is an inverse hexagonal mesophase of stiff consistency. D_2O was obtained from Merck and is quoted to be 99.75% isotopically pure. *n*-decane was obtained from Merck (> 99.0%).

Sample preparation. Samples were prepared by weight, first dissolving AOT in the oil at an elevated temperature, then brine was added. The NaCl concentration, $\epsilon = 0.6$ wt%, was kept fixed for all experiments.

Phase diagram determination. The phase diagrams were found to be most conveniently studied by starting at high γ and diluting with brine and oil at constant α. For a given composition the number and type of phases was determined visually in a thermostated water-bath. Crossed polarizers were used to detect anisotropic mesophases. This procedure yields sections through the phase prism (see Fig. 4, left). From these sections the other diagrams can be constructed.

Electrical conductivity measurements. The conductivity was measured using a Wayne Kerr Autobalance Brigde (B 905) operating a 1 kHz. The cell constant $a = 0.736\ \text{cm}^{-1}$ was determined using 0.01D KCl. A steep conductivity increase, irrespective of whether the solutions were stirred or not, with increasing temperature was observed (see Fig. 7 below).

SANS measurements. Small angle neutron scattering experiments were performed at the Biology Low Angle Diffractometer located at the beam port 9HB of the High Flux Beam Reactor of Brookhaven National Laboratory. Neutron beam was derived from an in-pile liquid hydrogen cold source. After going through a Be-filter and multilayer monochromator the average wavelength of neutron can be selected either at $\lambda = 4.5$ or 6.4 Å, with a relative wavelength spread $\Delta\lambda/\lambda$, of 9%. A series of pinholes of diameters, 10 mm/8 mm/6 mm over the distance of 2 m, were used to collimate the incident neutrons. Sample holders used were flat quartz cells of 1 mm path length. Scattered neutrons were detected by a rectangular 50×50 cm He^3 gas proportional counter with 256×256 pixels. With suitable choices of sample-to-detector distance, a Q-range of 0.01 to 0.25 Å^{-1} was covered in the measurements without having to change the detector distance. $Q = 4\pi \sin(\theta/2)/\lambda$ is the Bragg wave number of scattered neutrons at scattering angle θ. A standard data correction procedure was used.[25] The normalization to an absolute cross section was made by comparing the intensity with that of a 1 mm H_2O sample. In this paper we call $I(Q)$ a normalized intensity which is the scattering cross section per unit illuminated sample volume, having a unit of cm^{-1}. For a one-phase microemulsion we deal with in this article, we can check the measured absolute cross section in an alternative way by using a general invariant relation,

$$(\rho_{D_2O} - \rho_{C_{10}})^2 2\pi^2 \phi_w (1 - \phi_w) = \int_0^\infty Q^2 I(Q) dQ, \qquad (1)$$

where ρ_{D_2O} and $\rho_{C_{10}}$ are, respectively, the scattering length densities of heavy water and decane, and ϕ_w is the volume fraction of the aqueous phase (volume fraction of D_2O plus the volume fraction of the AOT headgroups).

III. PHASE BEHAVIOR

The phase behavior of quaternary mixtures, water–oil–ionic amphiphile–inorganic electrolyte, is determined by the phase diagrams of the corresponding binary and ternary mixtures. Since the details of the phase behavior have been described in a recent review article[20] we shall confine our-

selves here to a brief description of its features pertinent to this article.

The phase behavior of the ternary water–oil–amphiphile system is appropriately discussed by considering the respective binary systems first. Water and decane are of course practically immiscible over the considered temperature range. The binary system *n*-decane–AOT shows a complete miscibility between the melting and the boiling point of decane. Considerations based on analogy with other ionic amphiphile systems indicate that the binary system, water–AOT, shows a lower miscibility gap with an upper consolute point located *below* the melting point. Furthermore, a lamellar phase extends to low amphiphile concentrations covering the binary miscibility gap.

Proceeding to the ternary system water–*n*-decane–AOT, one finds in the isothermal Gibbs phase triangle the central water–*n*-decane miscibility gap with the critical point facing the *n*-decane–AOT side. Without added electrolyte the lamellar phase extends from the water side into the phase prism intersecting with the central miscibility gap. The position of the plait point near the *n*-decane–AOT side indicates tie lines of the central miscibility gap decline towards the oil corner. The lamellar phase, or more generally, tielines with one of the phases being the lamellar phase, extend towards the oil corner. This phase behavior is little affected by raising the temperature although AOT becomes more water soluble at higher temperatures. If, however, water is replaced by brine, that is if one proceeds to the quaternary system water–*n*-decane–AOT–NaCl, the situation changes dramatically.

A four-component system is appropriately discussed in three dimensions in a phase tetrahedron at constant temperature. If one wants to keep the temperature as variable one has to dispense with one of the composition variables, e.g., by keeping the ratio between two of them constant. The appropriate choice for the present work was to introduce the fraction of salt in the brine ϵ (in wt%). The phase behavior can then be discussed schematically in a pseudoternary phase prism shown in Fig. 1. Although the representation is not exact, this has no influence on the present discussion. The main effect of the electrolyte is—at ambient temperature—to push back the lamellar phase and drive the amphiphile into the oil-rich phase.[20,26,27] This situation is represented in the bottom triangle in Fig. 1 (we have omitted the lamellar phase for clarity). Increasing temperature leads to a better solubility of the ionic amphiphile in water. As a consequence, at the lower temperature T_l the oil-rich microemulsion splits into an oil-rich and an amphiphile-rich phase C of the three-phase body. Oil-rich phase moves with increasing temperature towards the oil corner whereas the amphiphile-rich phase C moves on an ascending trajectory towards the water-rich side. At the upper temperature T_u of the three-phase body, the amphiphile-rich C and the water-rich phase merge. Thus, a sample containing equal volumes of water, oil, and an appropriate amount of ionic amphiphile will show the phase sequence $\bar{2}$, 3, $\underline{2}$ with increasing temperature shown schematically in the test tubes on the right of Fig. 1. In Fig. 2 the actual phase diagram is shown for the system D_2O ($\epsilon = 0.6$ wt% NaCl)–*n*-decane–AOT, at a temperature of $T = 40$ °C.

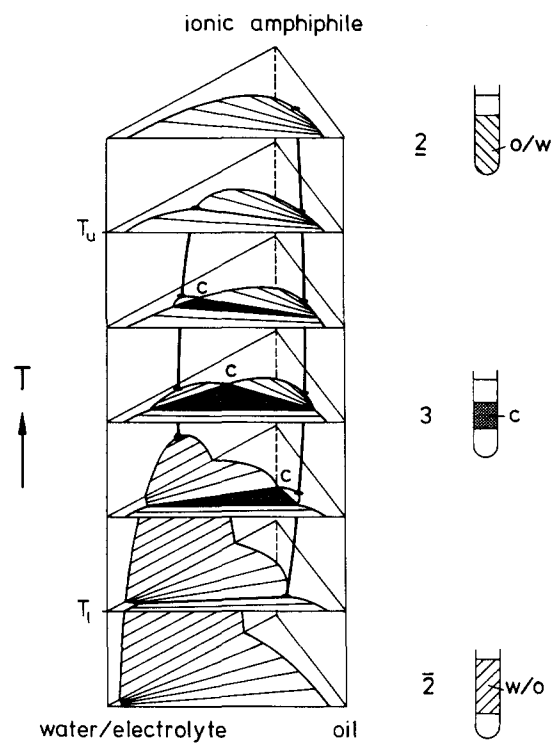

FIG. 1. The phase prism of water (electrolyte)/oil/ionic amphiphile in a pseudoternary representation. The series of diagrams shown in the constant temperature sections illustrate the progression from a water-in-oil microemulsion, ($\bar{2}$) in coexistence with an aqueous phase below the temperature T_l successively, though a three-phase coexistence (3) region with the amphiphile rich phase C in equilibrium with excess water and oil at intermediate temperature range, $T_u - T_l$, to an oil-in-water microemulsion ($\underline{2}$) in coexistence with an oil phase above the temperature T_u. Note the movement of the amphiphile-rich phase C from the oil-rich side at low temperatures to the water-rich side at high temperatures, characteristic of microemulsions made of ionic amphiphiles.

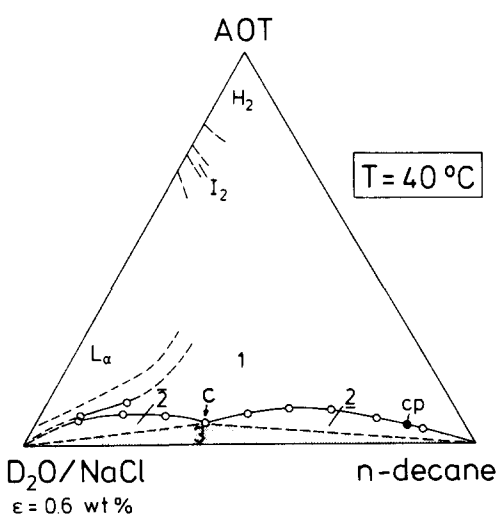

FIG. 2. Gibbs phase triangle of a system D_2O (0.6% NaCl)/*n*-decane/AOT at $T = 40$ °C. Note at the hydrophilic–hydrophobic balance temperature, the amphiphile-rich phase C contains approximately equal volumes of oil and water volume ratio ($\alpha = 40$). Without addition of salt, the amphiphile-rich phase C cannot be realized in the accessible temperature range.

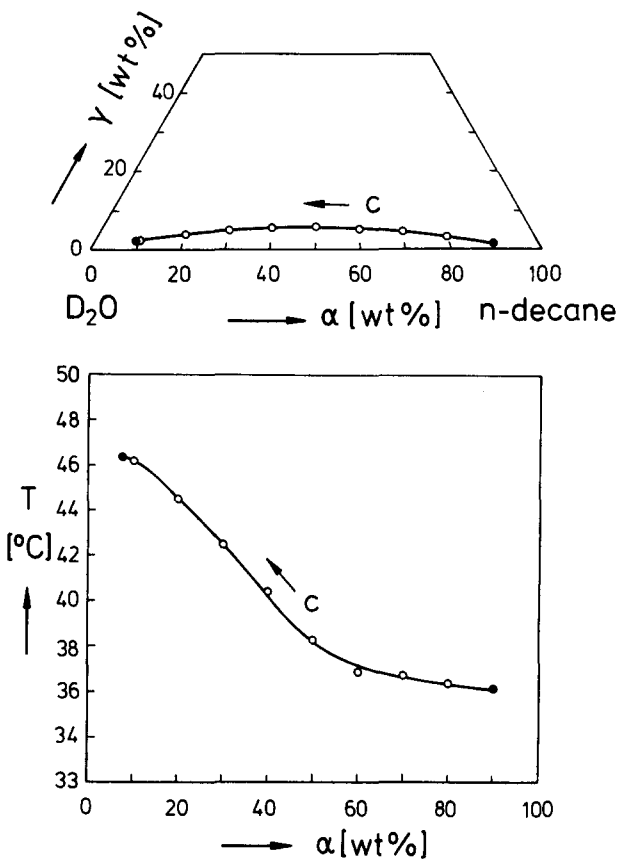

FIG. 3. Trajectory of the amphiphile-rich phase C as the temperature is raised. The upper diagram is the projection of the trajectory on to the $\alpha - \gamma$ plane of the phase prism. The bottom diagram is the movement of the trajectory in the $T - \alpha$ plane.

The trajectory of the amphiphile-rich phase C (a rather special point in the phase diagram) for the system D_2O ($\epsilon = 0.6$ wt% NaCl)–n-decane–AOT with increasing temperature is shown on Fig. 3. The projection of the trajectory onto the bottom plane of the phase prism is shown on the top of Fig. 3, the projection onto the T–water–oil plane on the bottom of Fig. 3. We found it convenient to introduce two compositional variables, α for the oil fraction (in water plus oil) and γ for the amphiphile weight fraction (in water + oil + AOT).

The data points in Fig. 3 were obtained by determining the occurring phases keeping α constant and varying γ, that is performing vertical sections through the phase prism. Such a section is shown for $\alpha = 40$ wt% on Fig. 4, left. While at low γ, there is only a narrow one-phase temperature gap, at higher γ, a much larger temperature gap can be observed.

From sections with different α, the phase boundaries of the one-phase channel were constructed for a constant AOT weight fraction of $\gamma = 12$ wt%, and shown in Fig. 4, right. From the comparison of Fig. 3, bottom, and Fig. 4, left, it is evident that the high mutual solubility of water and oil, mediated by the amphiphile, is intimately related to the trajectory of the amphiphile-rich phase C on the surface of the body of heterogeneous phases. Accordingly, proceeding from the lower right hand corner of Fig. 4, right, that is $\alpha = 90\%$, and lower temperature, to the upper left hand corner that is $\alpha = 10\%$, and higher temperature, an inversion from a water-in-oil to an oil-in-water microstructure may be anticipated.

IV. ANALYSES OF SANS RESULTS

In order to present the overview of the microstructure as seen from SANS experiments, we recast the one-phase channel depicted in Fig. 4, right, into a schematic representation of the overall feature as shown in Fig. 5. We have drawn into the one-phase channel an "artistic view" of the possible microstructure we visualize as a result of SANS data analyses. It is helpful to keep this picture in mind as the readers read the following paragraphs. In this picture, the shaded regions represent oil, and the rest of the white regions represent water. The upper two-phase region is denoted by $\underline{2}$ because the surfactant-rich microemulsion is on the bottom of the test tube coexisting with a predominant oil phase on the top. Thus, deep into the $\underline{2}$-phase region, the microemulsion is

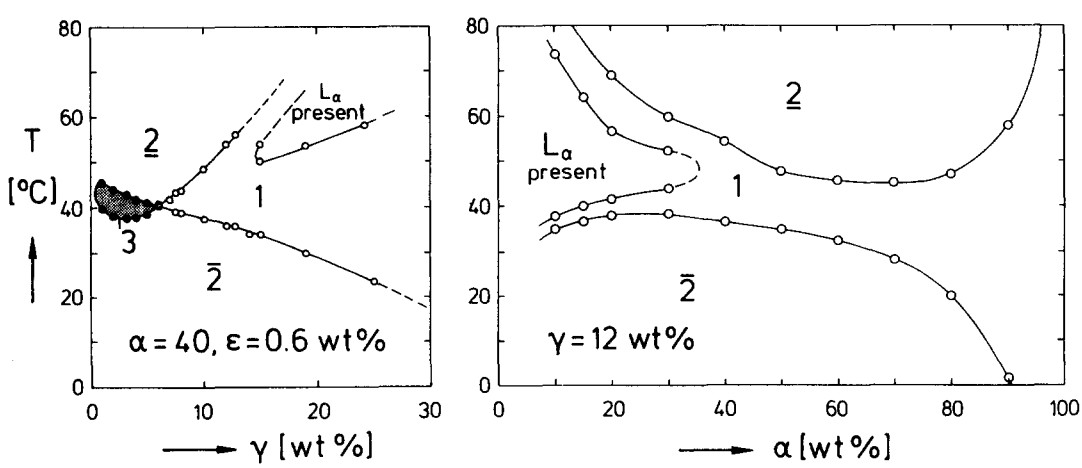

FIG. 4. Two sections through the body of heterogeneous phases in the phase prism. The left diagram is a section at $\alpha = 40$ (equal oil and water volumes) showing the relative positions of 3, $\bar{2}$, $\underline{2}$, and 1 phases in the $T - \gamma$ plane. The right diagram shows the one-phase channel which exists in the $T - \alpha$ plane at $\gamma = 12$. It is worthy to note that on the low α side, the one-phase channel splits into an upper and lower channels, intervened by a L_α phase in the intermediate range.

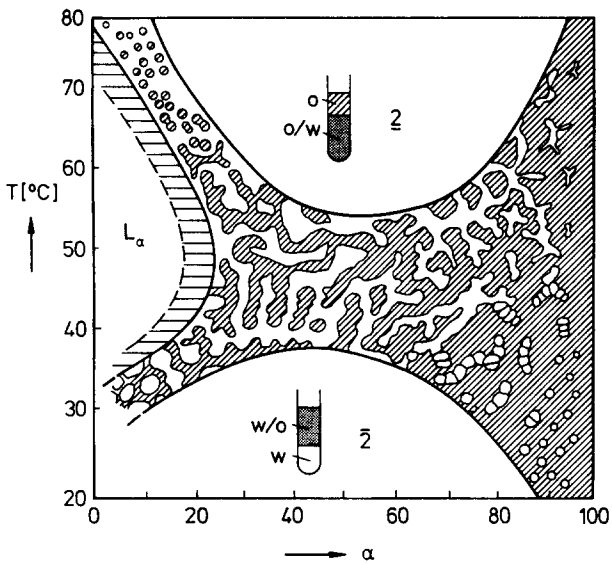

FIG. 5. Amplification of Fig. 4 right, for an illustration purpose. We draw onto the one-phase channel our conception of the microstructure as deduced from SANS data analysis. The shaded regions represent oil and the white regions represent water. The structure shown in the lower channel at $\alpha = 10$ and 20 is schematic only. Our SANS analysis only addresses the question of the average distances between water domains. Likewise for the upper channel, the analysis shows that the average distance between oil domains decreases as compared to that of the water domains in the lower channel.

likely to be of the o/w-type, because it expels an increasingly large amount of oil to the top phase as temperature increases. On the other hand, the lower two-phase region is denoted by $\bar{2}$ because the surfactant-rich microemulsion is the top phase in coexistence with a water-rich phase of higher density on the bottom. The microemulsion on the top is likely to be the w/o-type because it expels an increasingly large amount of water to the bottom phase as temperature decreases. We thus have an intuitive deduction that a structural inversion from w/o-type to o/w-type must have happened within the one-phase channel or possibly, not far from the two-phase boundaries.

It is natural to speculate that this inversion process is not ubiquitous as the oil content α varies from low to high. At the lower end, when $\alpha = 15$ or 20 %, the one-phase channel is split into two branches, an upper one and a lower one, by an intervening lamellar phase (L_α). The surfactant film curves toward water in the lower channel, but it curves toward neither water nor oil in the lamellar phase. It is therefore very plausible that it curves toward oil in the upper channel. We stated earlier, that an AOT head group becomes more hydrophilic as temperature rises. According to the Bancroft rule[28] then, it will prefer to face an exterior water at higher temperatures. On the other hand, at the higher end, say $\alpha = 80$ and 90 %, the water content of the microemulsion is low so that the inversion process could take place through an entirely different route. Here we shall see that there is a striking electrical conductivity percolation phenomenon as a function of temperature. The percolation temperatures for $\alpha = 80\%$ and $\alpha = 90\%$ occur around 35 °C, one-third from the lower boundary of the one-phase channel. Somehow the water droplets well separated at low temperatures must cluster to promote the conductivity. In the middle range of the oil-to-water weight ratio, say at $\alpha = 40$, where there is an equal volume of oil and water, the mean curvature of the surfactant film must be zero. This is because the one-phase channel is adjacent to the three-phase body, signifying that the surfactant molecule is balanced towards both oil and water, at this range of temperature. The microstructure is thus likely to be bicontinuous.[29] These qualitative speculations will be substantiated in the following paragraphs, in sequence.

A. Interpretation of low α data (α=15% and 20%)

SANS intensity distribution $I(Q)$ shows a single peak at both low and high temperatures within the one-phase channel for $\alpha = 15$ and 20 %. The characteristic feature of the peak is that at low temperatures the peak height $I(Q_m)$ is higher and the peak position Q_m lower. At higher temperatures the $I(Q_m)$ decreases while the Q_m increases. $I(Q)$ vs Q plots are shown for the two temperatures in Fig. 6 for the

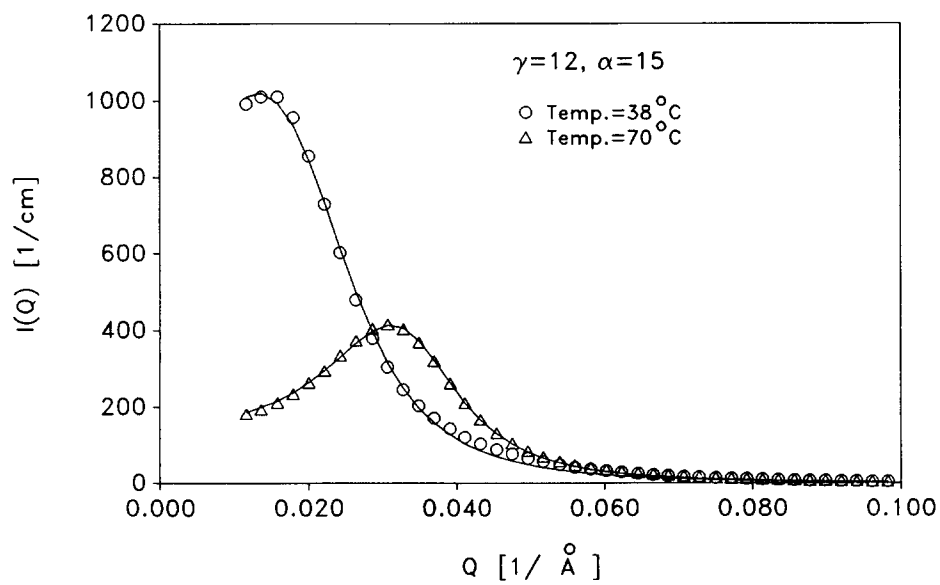

FIG. 6. SANS data, $I(Q)$ vs Q, for $\alpha = 15$, $T = 38$ °C (circle), and $T = 70$ °C (triangle), taken, respectively, at lower and upper channels. The solid lines are fittings using the Teubner–Strey model. For this low α region, the fitting of the model is only used to extract Q_m of the curves. We obtain $Q_m = 0.0136$ Å^{-1} for the first case (circle) and $Q_m = 0.310$ Å^{-1} for the second case (triangle). Note the substantial shift of the peak to larger Q value upon raising the temperature.

TABLE I. Analysis of a low α data.[a]

α	ϕ_w	Δ_H (Å)	Δ_L (Å)	$Q_m(L)/Q_m(H)$	$Q_m(w/o)/Q_m(o/w)$
15	0.718	7.3(70 °C)	7.6(38 °C)	0.44 ± 0.09	0.52 ± 0.02
20	0.662	7.6(61 °C)	7.5(39 °C)	0.50 ± 0.11	0.64 ± 0.03
40	0.461	8.1(52 °C)	8.0(40 °C)	0.82 ± 0.20	1.13 ± 0.04

[a] $\phi_w = \phi_{D_2O} + \phi_H = \phi_{D_2O} + \frac{65}{611}\phi_s$.

$\alpha = 15$ case. The reason that the peak height decreases when Q_m shifts to higher value can be easily understood by referring to Eq. (1). Since by changing the temperature the quantity on the left hand side of the equation does not change, the integral of $Q^2I(Q)$ over the entire range of the curve is an invariant. Therefore the higher the value of Q_m the lower the peak height is. Based on the observation that Q_m shifts to a higher value as the temperature is jumped, we can demonstrate that the microemulsion must transform from a water-internal structure at low temperatures to an oil-internal structure at high temperatures, because in doing so the interdroplet separation decreases.

Under assumptions that the oil (or water) domains in the microemulsion are spherical in shape, having a single layer of surfactant coating, and the domains arrange themselves locally in a liquidlike structure, the ratio of the Q_m in the w/o microemulsion (low temperature) to that in the o/w microemulsion (high temperature) can be shown to be given by the following formulas:[3]

$$\frac{Q_m(\text{w/o})}{Q_m(\text{o/w})} = \left[\frac{1-\phi_w}{\phi_w}\right]^{2/3}\frac{\Delta_H}{\Delta_L}, \tag{2}$$

where ϕ_w is the volume fraction of the aqueous phase (i.e., the volume fraction of D_2O plus the volume fraction of the AOT head groups). Δ is a geometrical constant of the surfactant molecule defined as $\Delta = v_s/a_h$, where v_s and a_h are, respectively, the steric volume of the surfactant molecule and the available area for the head group in the packing. The subscript H and L mean, respectively, the high and low temperature cases. Values of Δ_H and Δ_L are determined separately from analyses of the large Q portion of $I(Q)$ as described in Sec. IV D. We note here only that Δ is related to the specific surface area per unit volume by a relation, $\Delta = \phi_s(S/V)^{-1}$. The required volume fractions can be computed from α and γ by using the known values of the densities, $\rho_{D_2O} = 1.105$ g/cm^3, $\rho_o = 0.73$ g/cm^3, and $\rho_s = 1.15$ g/cm^3 of heavy water, decane, and AOT, respectively.

Table I gives the experimentally determined Δ_H, Δ_L, and $Q_m(L)/Q_m(H)$ in the 3rd, 4th, and 5th columns, respectively. The calculated ratio $Q_m(\text{w/o})/Q_m(\text{o/w})$ according to Eq. (2) is given in the sixth column. We see from the table that the agreement between the experimental $Q_m(L)/Q_m(H)$ and the theoretical $Q_m(\text{w/o})/Q_m(\text{o/w})$ is satisfactory within the experimental errors for the cases of $\alpha = 15\%$ and $\alpha = 20\%$. On the other hand for the $\alpha = 40\%$ case the agreement is not as good, indicating that the assumption of the water droplets picture for this case is not as good. The solid lines in Fig. 6 are the fitted curves using Teubner–Strey model[36] to be described in the next section. In the context of this section, the model fits are only used to determine more accurately the position of Q_m.

B. Interpretation of high α data

In contrast to the low α data, $I(Q)$ for $\alpha = 80$ and 90 % show no peaks. The intensity increases monotonically towards $Q = 0$. In a $\log I(Q)$ vs $\log Q$ representation the curve displays two distinct slopes, a gentle one for low Q region and a steeper one for high Q region. This type of intensity distribution is reminiscent of scattering from a polymerlike object.[31] One can imagine a polymerlike string of microemulsion droplets clustered together by an attractive force. Or alternatively one might have a fractal aggregate of these droplets.[31,32] This is an idealization of a complex positional correlations of the droplets as seen in a snap shot. The static structure factor as measured by SANS corresponds to a Fourier transform of this snap shot. To support this hypothesis we measured the electric conductivity κ as a function of temperature for three cases with $\alpha = 70$, 80, and 90 %. The results are plotted in $\log \kappa$ vs T in Fig. 7. One sees a familiar percolation behavior with a percolation temperature T_p at around 35 °C.[6–10] This temperature is situated in the one-phase region at about one-third from the lower two-phase boundary (see Fig. 5). Apparently extensive electrically conducting pathways are formed upon increasing temperatures beyond T_p. Kim and Huang[7] proposed that in the AOT–decane–water system the conduction may be mediated by hopping of surfactant molecules from droplet to droplet when they approach within certain distance. This process is termed a dynamic percolation.[32] We shall adopt this picture for the interpretation of the scattering results. Comparison of the high temperature end of the conductivity curves with the conductivity of pure brine at the respective temperature suggests that the conducting pathways convert themselves from chain of droplets at and below the percolation temperature into an extended network of water channels at high temperatures.[16] The scattering pattern, with water–oil contrast, of the network is probably indistinguishable from chains of droplets.

The normalized scattering intensity for a system of correlated w/o microemulsion droplets may be written as

$$I(Q) = (\rho_{D_2O} - \rho_{C10})^2\phi_w\frac{4\pi}{3}\frac{\langle R^6\rangle}{\langle R^3\rangle}\frac{\langle R^6\overline{P}(QR)\rangle}{\langle R^6\rangle}S(Q), \tag{3}$$

where ρ_{D_2O} and ρ_{C10} are, respectively, the scattering length densities of D_2O and decane, R is the radius of the water pool and $\overline{P}(QR) = [3j_1(QR)/QR]^2$ is the particle struc-

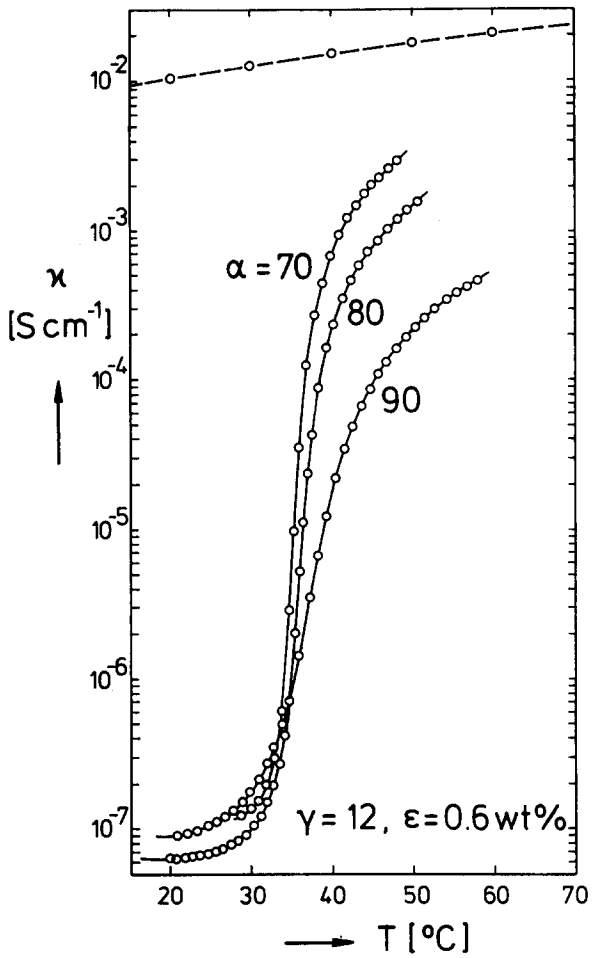

FIG. 7. Electrical conductivity of one-phase microemulsions as a function of temperature at $\alpha = 70$, 80, and 90. Note the rapid increase in κ near $T = 35$ °C (by 3 to 4 orders of magnitude) indicating percolation behavior due to the change in the microstructure. Note the conductivity of pure brine ($\epsilon = 0.6$ wt%) indicated by the dashed line.

ture factor of a sphere of radius R, and $S(Q)$ is the interdroplet structure factor. The brackets denote the size averaged over a size distribution function (Schultz distribution).

$$f_R(R) = \left[\frac{Z+1}{\bar{R}}\right]^{z+1} \frac{1}{\Gamma(Z+1)} R^z \times \exp\left[-\left(\frac{Z+1}{\bar{R}}\right)R\right]. \quad (4)$$

$\bar{R}$ in Eq. (4) denotes the average radius $\langle R \rangle$ and Z is an index specifying the dispersion. The size polydispersity is given by $p = \Delta R/\bar{R} = (1+Z)^{-1/2}$. For the Schultz distribution the ratio $\langle R^6 \rangle / \langle R^3 \rangle$ has a value

$$\frac{\langle R^6 \rangle}{\langle R^3 \rangle} = \bar{R}^3 \left[\frac{(Z+6)(Z+5)(Z+4)}{(Z+1)^3}\right]. \quad (5)$$

but for a rectangular distribution the bracket in the above equation is unity.

The Structure Factor $S(Q)$. We imagine that as we raise the temperature the water droplets begin to cluster and form chainlike objects. If the centers of spheres are located at $\underline{R}_j$, and there are N spheres in each chain then

$$S(Q) = 1 + \frac{1}{N}\left\langle \sum_{j \neq k}^{N} \exp[i\underline{Q}\cdot(\underline{R}_j - \underline{R}_k)] \right\rangle. \quad (6)$$

To evaluate $S(Q)$, one first makes a Gaussian approximation[33] and then writes $\langle |R_{jk}|^2 \rangle = L^2 |j-k|^{2/D}$, where L is the interparticle distance along the chain and D the fractal dimension of the aggregates. One finally arrives at a result[31]

$$S(Q) = 1 + \frac{2}{N}\sum_{n=1}^{N} (N-n)\exp\left[\frac{1}{6}Q^2L^2n^{2/D}\right]. \quad (7)$$

The sum in Eq. (7) can be calculated term by term numerically for any arbitrary N. The pertinent behavior for the structure factor in different Q-ranges is as follows:

(i) For small values of Q where $QR_g < 1$, one has a Guinier region and $S(Q) \simeq N \cdot \exp[-Q^2R_g^2/3]$, and the radius of gyration is given by

$$R_g^2 = L^2N^{2/D}\left[2\left(1+\frac{1}{D}\right)\left(1+\frac{2}{D}\right)\right]^{-1}. \quad (8)$$

This small Q range is beyond our reach in this experiment.

(ii) For an intermediate Q range where $QR_g > 1$ and $QL \sim 1$, one has a fractal region and

$$S(Q) \simeq 1 + D\,6^{D/2}\Gamma\left(\frac{D}{2}\right)(QL)^{-D}. \quad (9)$$

(iii) For large Q where $QL \gg 1$, $S(Q) \to 1$, and one has the single particle region.

Putting Eq. (7) back into Eq. (3), we can describe the behavior of $I(Q)$ vs Q as follows: Since $R < L \approx 140$ Å, we do not observe the small Q range. In the intermediate Q range, where 0.01 Å^{-1} $< Q <$ 0.05 Å we have a fractallike scattering, $I(Q) \approx (QL)^{-D}$, so a $\log I(Q)$ vs $\log Q$ plot would show approximately a slope $-D$. In the large Q range where $Q > 0.1$ Å, $S(Q) \to 1$, one sees the large Q behavior of $\bar{P}(QR)$ function (or its polydisperse average) so $\log I(Q)$ vs $\log Q$ plot shows a slope of -4.

Figure 8 shows results of analyses using Eq. (3) for the case $\alpha = 90\%$ at three temperatures 36, 44, 54 °C (from the bottom up). Symbols are the experimental data and solid

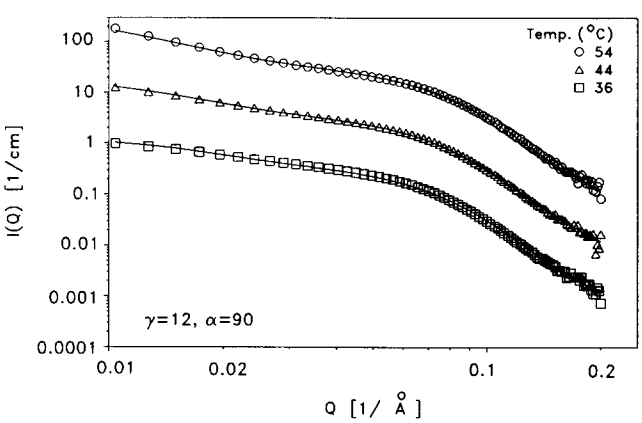

FIG. 8. SANS data of microemulsions at high α. Curves are for $\alpha = 90$, successively from top to bottom, $T = 54$ °C (circle), $T = 44$ °C (triangle), and $T = 36$ °C (square). Note $I(Q)$ vs Q curves show no peak. In this $\log I(Q)$ vs $\log Q$ representation, there are two distinct slopes, the first one is approximately the $-D$ (about -1.7) and the second one -4. The solid lines are theoretical fits (in absolute unit) using the polymerlike chain model described in the text.

TABLE II. Analysis of high α data.

	$\alpha = 90$		
	$T = 36$ °C	$T = 44$ °C	$T = 54$ °C
N	3	5	13
D	1.7	1.7	1.7
R (Å)	24.7	24.5	24
Z	10	10	10
L (Å)	140	140	140
Rg (Å)	101	137	241

lines are the theory. Results for the case $\alpha = 80\%$ are qualitatively similar. Agreement between the experimental absolute intensities and the theoretical calculations is quantitatively good. The parameter extracted from the fits are given in Table II.

Independent parameters of the theory are $\bar{R}$ and Z for $\bar{P}(Q)$ and N, L, D for $S(Q)$. $\bar{R}$ and Z give the mean size of the droplets and its size distribution, N and L give the average number of microemulsion droplets in a chain and the separation between the droplets; D is the fractal dimension which should be 1.7 for polymerlike objects. We set $Z = 10$ which corresponds to 30% polydispersity known to exist in AOT microemulsions.[3] L is found to be 140 Å for the best overall fittings. $\bar{R}$ is approximately 24 Å, from the known water to surfactant molar ratio. The value of D is fixed at 1.7 assuming that the conformation of the chains is on the average Gaussian. Thus the only variable of the fit is N. Looking at Table II one sees that as the temperature increases N increases from 3 at 36 °C, to 5 at 44 °C and to 13 at 54 °C, showing the tendency for droplets to cluster. The value of L of 140 Å is unexpectedly large for the average size $2\bar{R}$ of 50 Å. This is probably because we are idealizing a complicated spatial arrangement of nonspherical particles by a chain of spherical particles arranged with a uniform spacing L. It could also mean that a conduction pathway can be formed when two microemulsion droplets approach to a distance less than 140 Å. Nevertheless the trends of parameters listed in Table II are in the right direction for the dynamic percolation to occur at elevated temperatures.

C. Interpretation of $\alpha = 40$ data

At $\alpha = 40\%$, the volume fractions of oil and water are nearly equal ($\phi_{D_2O} = 0.451$, $\phi_0 = 0.455$). Since the AOT molecule, in the one-phase temperature range, is nearly balanced with respect to its hydrophilicity and hydrophobicity, the surfactant film, in the equal oil–water volume fraction case, would like to adopt a configuration of zero mean curvature. The microstructure is thus likely to be bicontinuous. This conjecture is somewhat supported by the fact that the droplet picture does not predict correctly the shift of the peak in SANS data from low to high temperatures, for the case of $\alpha = 40$, listed in Table I. Since a bicontinuous structure is a disordered structure consisting of interpenetrating oil and water microdomains, a natural description of it in real space is in terms of the scattering length density fluctuation correlation function introduced by Debye and Bueche.[34] $\Gamma(\underline{r}) = \langle \eta(0)\eta(\underline{r})\rangle / \langle \eta^2 \rangle$. $\eta(\underline{r})$ is the deviation of the scattering length density at $\underline{r}$ from the mean value $\bar{\rho} = \phi_w \rho_{D_2O} + (1 - \phi_w)\rho_{C10}$. It is easily shown that $\langle \eta^2 \rangle = \phi_w (1 - \phi_w)(\rho_{D_2O} - \rho_{C10})^2$. $\Gamma(\underline{r})$ has three basic properties:[35] $\Gamma(\underline{r})$ is a function of scalar r with $\Gamma(0) = 1$ and $\Gamma(\infty) = 0$, and the initial slope satisfies a relation

$$\Gamma'(r = 0) = -\frac{1}{4\phi_w(1 - \phi_w)} \frac{S}{V}, \tag{10}$$

where S/V is the interfacial area per unit volume of the sample. The normalized scattering intensity can be written as a three dimensional Fourier transform of $\Gamma(\underline{r})$, i.e.,

$$I(Q) = \langle \eta^2 \rangle \int_0^\infty dr\, 4\pi r^2 \frac{\sin Qr}{Qr} \Gamma(r). \tag{11}$$

Debye formalism has been used for analyses of scattering data from bicontinuous microemulsions by Auvray *et al.*[22] and de Geyer *et al.*[23] These microemulsions were all taken from the middle phase (the surfactant-rich phase) of five-component microemulsions containing alcohol and salt. More recently Teubner and Strey,[36] Vonk *et al.*[37] and Ninham *et al.*[38] have separately proposed different structural models for constructing $\Gamma(r)$, for the purpose of analyzing scattering data from three-component and five-component microemulsions. In this section we shall use the models of Teubner and Strey and of Vonk *et al.* for the analysis of our data, since the two models are very similar.

In the case of a bicontinuous microemulsion, the mixture of oil and water cannot be completely random because there is a monolayer of surfactant film in between an oil domain and a water domain. The surfactant monolayer, having a finite bending elastic constant, would not allow either the oil domain or the water domain to become too small. In fact a recent freeze fracture electron microscopy picture of a ternary nonionic microemulsion (H_2O–*n*-octane–$C_{12}E_5$) showed that at 50/50 oil to water volume ratio there exist interpenetrating water and oil domains.[39] These domains are approximately tubular in shape having a fairly well defined diameter. Since we used D_2O instead of H_2O, for SANS measurements, and D_2O has much higher scattering length density compared to oil, a large and positive contribution will be made to $\Gamma(r)$, if the chord length r spans two water domains or two oil domains. If we fix the origin, say, at a water domain and draw a radial chord outward, the end of the chord will meet another water domain in, more or less a periodic way. Let this period be denoted by d and putting $k = 2\pi/d$. The well-known Debye correlation function for porous media, $\exp(-\lambda r)$,[35] would have to be modified, in the first approximation, by multiplying by an isotropically averaged periodic factor $\langle e^{i\underline{k}\cdot\underline{r}} \rangle$, which is equal to $j_0(kr)$. Thus one can assume

$$\Gamma(r) = j_0(kr) \cdot \exp(-\lambda r). \tag{12}$$

This expression has been derived by Teubner and Strey[36] from a consideration of a Landau expansion of the free energy functional of a microemulsion system. We note that from Eq. (12) $\Gamma'(r = 0) = -\lambda$, therefore combining this expression with Eq. (10), we see that, the parameter λ is related to the specific surface area of the surfactant film. The parameter $d = 2\pi/k$ can be interpreted as the average distance between the water domains or oil domains.

Substituting Eq. (12) into Eq. (11) we get, for the scattering intensity,

$$I(Q) = (\Delta\rho)^2 \frac{2\pi S/V}{a^2 - 2Q_m^2 Q^2 + Q^4}, \tag{13}$$

where $\Delta\rho = \rho_{D_2O} - \rho_{C10}$ is the water–oil contrast known to have a value 7.1×10^{10} cm^{-2}. The two constants in the denominator are given, respectively, by $a^2 = (k^2+\lambda^2)^2$, $Q_m^2 = k^2 - \lambda^2$ and Q_m has the meaning of the peak position of $I(Q)$.

A variation of the Teubner–Strey model given above was suggested by Ciccariello and Benedetti,[40] and has been applied to interpret light scattering intensity distribution from polymer blends undergoing phase separation by Wang *et al.*[41] This is the one-dimensional version of the Teubner–Strey model and it amounts to replacing the first factor in Eq. (12) by the one-dimensional sinusoidal function, $\cos(kr)$. The intensity function is, in this model,[41]

$$I(Q) = (\Delta\rho)^2 \pi \frac{S}{V}\left(\frac{1+k/Q}{[\lambda^2+(Q+k)^2]^2} + \frac{1-k/Q}{[\lambda^2+(Q-k)^2]^2}\right). \tag{14}$$

In this expression the parameter λ is still given by Eq. (10). The meaning of k is the same as before which is equal to $2\pi/d$.

The third model we used in this analysis was due to Vonk, Billman, and Kaler.[37] In this model the authors assumed that the microstructure of a bicontinuous microemulsion can be taken as that of a distorted lamellar structure with alternating water and oil layers separated by monolayers of surfactant films. We shall not go into details of the description of it because it has already been given in Ref. 37. The resultant $\Gamma(r)$ function contains, besides an exponential factor like that in Eq. (12), a damped sinusoidal factor constructed from a one-dimensional correlation function $\gamma_1(x)$, i.e.,

$$\Gamma(r) = \frac{1}{r}\cdot\exp(-\lambda r)\int_0^r \gamma_1(x)dx. \tag{15}$$

This expression contains two parameters: a lamellar repeat distance D, which occurs in the expression for $\gamma_1(x)$, and $d = 2/\lambda$ which is the distortion length along the lamellar surface. We shall now present the results of these analyses in sequence.

Figure 9(a) shows log-linear plots of $I(Q)$ vs Q, at three temperatures, $T = 40, 46, 52$ °C (from top down), for a one-phase microemulsion with a composition $\gamma = 12$ and $\alpha = 40$. Symbols are SANS data and solid lines are theoretical analyses based on Teubner–Strey model.[36] The agreement in the peak region is very good judging from linear plots which are not shown here. The agreement in the tail region of the curves is seen to be good also. From these fits we extract a set of parameters, $k = 2\pi/d$ an $\lambda = 1/\xi$, the latter gives S/V value through the relation Eq. (10). In this model the peak position Q_m does not have a fundamental significance, since it is given in terms of a combination of k and λ.

Figure 9(b) gives the corresponding presentation of the results of analyses using the model of Wang *et al.*[41] Clearly

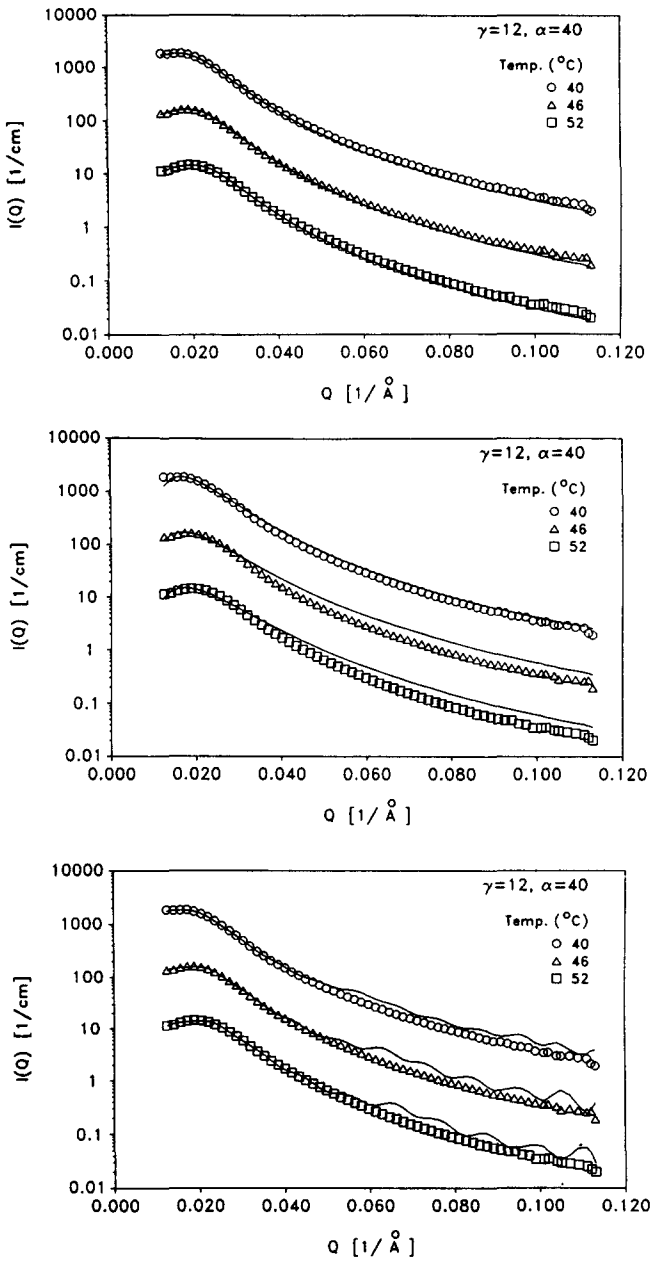

FIG. 9. Model analysis of $I(Q)$ vs Q curves for microemulsions having a composition $\alpha = 40$, $\gamma = 12$, at three different temperatures, $T = 40$ °C (circle), $T = 46$ °C (triangle), and $T = 52$ °C (square). The microemulsions at this composition have an equal oil-to-water volume ratio, so likely to be bicontinuous. The solid lines are result of analyses using the Teubner–Strey model (Ref. 36) (a), model of Wang *et al.* (Ref. 41) (b), and model of Vonk *et al.* (Ref. 37) (c).

the agreement is much inferior compared to the Teubner–Strey model.

Figure 9(c) gives the results of analyses using the model of Vonk *et al.*[37] The agreement is fair as compared to the model of Teubner and Strey. The oscillation of the theoretical curves at large Q can be damped out by introducing a polydispersity in the lamellar spacing D, as was done in Ref. 37. For a simple model like this an introduction of yet another parameter into the theory seems to be an excess. So we do not pursue it further. Results of all parameters extracted from the analyses based on the three models are summarized in Table III together with χ^2 of the fits. One particularly

TABLE III. Model of a microemulsion with $\gamma = 12$, $\alpha = 40$.

T(°C)	Teubner–Strey[36]	Wang *et al.*[40]	Vonk *et al.*[37]
40 °C	$k = 0.0190$ (Å^{-1}) $k\xi = 1.83$ $\chi^2 = 0.332$	$k = 0.0113$ (Å^{-1}) $a_0 = 74.9$ (Å) $\chi^2 = 4.811$	$D = 331$ (Å) $d = 196$ (Å) $\chi^2 = 1.752$
46 °C	$k = 0.0209$ (Å^{-1}) $k\xi = 2.12$ $\chi^2 = 0.244$	$k = 0.0114$ (Å^{-1}) $a_0 = 64.6$ (Å) $\chi^2 = 8.234$	$D = 300$ (Å) $d = 204$ (Å) $\chi^2 = 2.296$
52 °C	$k = 0.0218$ (Å^{-1}) $k\xi = 2.19$ $\chi^2 = 0.271$	$k = 0.0118$ (Å^{-1}) $a_0 = 61.7$ (Å) $\chi^2 = 8.419$	$D = 288$ (Å) $d = 200$ (Å) $\chi^2 = 2.371$
	$k = 2\pi/\mathrm{d}$, $\lambda = 1/\xi$	$\lambda = 1/a_0$	$\lambda = 2/d$

noteworthy point is that d parameter extracted from Teubner–Strey model is almost exactly equal to the lamellar repeat distance D extracted from Vonk *et al.* model. Likewise ξ in the Teubner–Strey model is closely equal to half of the distortion distance d in the model of Vonk *et al.* Thus, we can conclude that the two models are practically identical in its physical content.

D. Analyses of large Q data

So far we have focused attention only on the small Q region of $I(Q)$ where there is either a peak or a fractal scattering. Results of the analyses are therefore highly model dependent. We can, however, perform a model independent analysis of large Q region based on a theorem given by Porod[42] and Debye,[35] which states that, for a two-component system with sharp interfaces, there is an asymptotic relation:

$$\frac{S}{V} = \pi\phi_w(1-\phi_w)\lim_{Q\to\infty} Q^4 I(Q) \Big/ \int_0^\infty dQ\, Q^2 I(Q). \quad (16)$$

The area per AOT head group can then be calculated by a formula

$$a_H = \frac{S}{V}\frac{v_s}{\phi_s} = \frac{S}{V}\frac{611}{\phi_s}, \quad (17)$$

where $v_s = 611$ Å^3 is the monomer volume of AOT. In practice $Q\to\infty$ amounts to take $QL > \pi$ where L is the characteristic length of the system. We have evaluated a_H according to Eq. (17) for samples of different α measured in the one-phase channel. These values are given in Table IV along with the effective $[Na^+]$ ion concentration in the water domains. $[Na^+]$ is calculated from a formula

$$[Na^+] = [NaCl] + 0.25[AOT]$$
$$= 0.113 + \frac{0.0847}{1-\alpha}(\mathrm{mole/l}), \quad (18)$$

where we assume a constant 25% dissociation of the counterions.

V. DISCUSSION OF THE RESULTS

So far we have made use of only SANS data in arriving at the numerical conclusions listed in the series of Tables presented in the last section. However, in constructing the pictorial microstructure representation as depicted in Fig. 5, some literature results were taken into consideration.

On the low α side there was an NMR self-diffusion study of Carnali *et al.*[12] on a system, water (0.46% NaCl)–iso-octane–AOT. This study indicated that on the water-rich side, at high temperatures (inside the upper one-phase channel), isolated oil droplets turned into aggregates upon decreasing the temperature. Specifically the ratio of the self-diffusion coefficient of the oil in the microemulsion, D_o, to the self-diffusion coefficient of the bulk oil, D_b, was found to be 0.01 at the upper boundary of the upper one-phase channel, and this ratio increases to 0.1 at the lower boundary of the same channel. The ratio in the lower one-phase channel, however, increases even further to 0.4 to 0.5 indicating the presence of an oil-continuous microemulsion.

On the high α side there were reaction kinetic studies of Lang *et al.*[16] and electric conductivity studies of Eicke and co-workers.[9–11] These results supported the notion of an aggregation of water droplets into more extended fractallike

TABLE IV. Area per head group at $\gamma = 12$.

α	T (°C)	a_H (Å^2)	$[Na^+]$ (mol/l)
10	37	85	0.207
15	38	82	0.213
20	39	81	0.219
30	41	80	0.234
40	41	78	0.254
50	41	76	0.282
60	41	74	0.325
70	38	72	0.395
80	36	67	0.537
90	34	62	0.96

clusters. The fusion of the aggregates into a tubular network of conducting channels,[16] albeit a transient phenomenon, was also observed by freeze fracture electron microscopy on related systems by Jahn and Strey.[43] A more recent conductivity, viscosity, and Kerr effect studies by Borkovec *et al.*[9] supported a picture of two symmetric percolation processes occurring around $\alpha = 20$ and $\alpha = 80$. Our scattering data while consistent with this idea does not necessarily support the symmetric water and oil percolation picture. The asymmetry can be generated by the difference in double layers interaction energy in the reversed and normal micellar configurations.

The bicontinuous structure for the equal volumes of oil and water case has also been supported by NMR self-diffusion data of Carnali *et al.*[12] For the $\alpha = 40$ case they reported the self-diffusion constants of oil and water to be about $\frac{1}{2}$ of the bulk values. Our measurements give an evolution of this bicontinuous structure as a function of temperature in terms of the two parameters d and ξ.

One more significant quantity a_H has been deduced from our neutron data at high Q by a model independent analysis. The value of a_H varies from 85 for $\alpha = 10$ continuously down to 62 for $\alpha = 90$ (see Table IV) in agreement with the values reported by Aveyard *et al.*[14] However, the ionic strength is roughly twice as high in our case. This may be due to the fact that their head group areas were measured at flat interfaces while our head group areas are measured at curved interfaces and the charge condensation effect is different for the two cases.

VI. SUMMARY AND PROSPECT

In this paper we have addressed a simple question: Can a one-phase microemulsion have different microstructures depending on its temperature? The answer is definitely: "Yes." This means that a macroscopic, thermodynamic phase does not have to correspond to a single unique microstructure. A macroscopic phase is normally identified visually as a homogeneous, isotropic liquid layer when illuminating with optical wavelengths. But looking with neutrons of wavelengths 5 to 10 Å, the situation could be different. Even within a one-phase region, there is a continuous structural evolution and even structural inversion.

We have identified an appropriate microemulsion system, D_2O (0.6% NaCl)/n = decane/AOT, which has a wide one-phase channel at a convenient temperature range. Furthermore at a suitable surfactant concentration $\gamma = 12$, the one-phase region is close to the amphiphile-rich phase C and is bounded on the top and the bottom by $\underline{2}$ and $\overline{2}$ phase regions, respectively. We have studied the microstructure of the one-phase microemulsion as a function of the oil weight fraction α and at different temperatures.

In the limit of high water content, $\alpha = 15$ and 20, we relate the peak position of the SANS intensity distribution to the average interdroplet distance using surfactant volume and surface area conservation relations. Thus the peak position is given as different functions of the volume fraction of water, depending on whether the surfactant film is curved towards water or oil. From this analysis we infer that the microemulsion in the lower one-phase channel is water-internal and inverts to an oil-internal structure on the upper one-phase channel. This conclusion is reasonable in view of the fact that a lamellar phase occurs in between these two temperature ranges.

In the opposite limit of low water content, $\alpha = 80$, and 90, we infer from a percolation behavior of the electrical conductivity at a suitable temperature that the water droplets, which must exist in the lower $\overline{2}$ phase region, become clustered in the one-phase region. A structural model consisting of Gaussian chainlike water-droplet clusters is used to calculate SANS cross section. We find, as the temperature increases, the number of droplets in the chain increases. The water droplet size and size distribution are in the expected range.

For the case of equal oil-to-water volume fraction, $\alpha = 40$, we expect to obtain a bicontinuous microemulsion because at this one-phase temperature range, the hydrophilicity and hydrophobicity of the AOT molecule is well balanced. We therefore use various models for the scattering length density fluctuation correlation function to analyze SANS data. In particular the models of Teubner and Strey and of Vonk *et al.* are shown to describe the intensity distributions equally well. We extract two model parameters from these analyses, which give, respectively, the average intertubular distance of the water or oil domains, and the specific surface area of the surfactant film. An independent analysis of the large Q data for all α gives variation of the average head area per surfactant molecule as a function of α. We relate the variation to the effective ionic strength within the water domains.

In the next paper of this series we shall turn our attention to detailed analyses of $\alpha = 40$ data at various surfactant concentrations γ. We shall examine the applicability of geometrical models such as DOC model of Zemb *et al.*[38] and theoretical models for bicontinuous microemulsions such as Widoms model,[44] Gompper and Schick model,[45] and the model of Milner *et al.*[46]

ACKNOWLEDGMENTS

We are indebted to Professor M. Kahlweit for initiating and supporting this work. We also thank J. Winkler for help with the conductivity measurements, M. Teubner for valuable discussions, and C. F. Wu for performing some of SANS measurements at Brookhaven National Laboratory. We are grateful to B. Schoenborn and D. Schneider for providing us with the neutron facility and neutron beam time. Research work of S.-H. C. is supported by grants from National Science Foundation. In addition he gratefully acknowledges the financial support from Alexander Von Humboldt US Senior Scientist Award during the period, May 1987–July 1988, when the experimental part of this paper was undertaken.

[1] H. Kunieda and K. Shinoda, J. Coll. Interface Sci. **7**, 601 (1980).
[2] C. Cabos and P. Delord, J. Appl. Cryst. **12**, 502 (1979).
[3] M. Kotlarchyk, S.-H. Chen, J. S. Huang, and M. W. Kim, Phys. Rev. A **29**, 2054 (1984); M. Kotlarchyk, S.-H. Chen, J. S. Huang, and M. W. Kim, Phys. Rev. Lett. **53**, 941 (1984).

[4] B. H. Robinson, C. T. Toprakcioglu, J. C. Dore, and P. Chieux, J. Chem. Soc. Faraday Trans. 1, **80**, 13 (1984).
[5] S.-H. Chen, T. Lin, J. S. Huang, in *Physics of Complex and Supermolecular Fluids, Exxon Monograph*, edited by S. A. Safran and N. A. Clark (Wiley, New York, 1987).
[6] S. Bhattacharya, J. P. Stokes, M. W. Kim, and J. S. Huang, Phys. Rev. Lett. **55**, 1884 (1985).
[7] M. W. Kim and J. S. Huang, Phys. Rev. A **34**, 719 (1986).
[8] J. Peyrelasse, C. Boned, and G. Marin, Colloid Polymer Sci. **264**, 143 (1986).
[9] M. Borkovec, H.-F. Eicke, H. Hammerich, and B. Das Gupta, J. Phys. Chem. **92**, 206 (1988).
[10] R. Hilfiker, H.-F. Eicke, S. Geiger, and G. Furler, J. Colloid and Interf. Sci. **105**, 378 (1985).
[11] S. Geiger and H.-F. Eicke, J. Colloid Interf. Sci. **110**, 181 (1986).
[12] J. O. Carnali, A. Ceglie, B. Lindman, and K. Shinoda, Langmuir **2**, 417 (1986).
[13] R. Aveyard, B. P. Binks, S. Clark, and J. Mead, J. Chem. Soc. Faraday Trans. 1, **82**, 125 (1986).
[14] R. Aveyard, B. P. Binks, and J. Mead, J. Chem. Soc. Faraday Trans. 1, **82**, 1755 (1986).
[15] J. S. Huang, S. T. Milner, B. Farago, and D. Richter, Phys. Rev. Lett. **59**, 2600 (1987).
[16] J. Lang, A. Jada, and A. Malliaris, J. Phys. Chem. **92**, 1946 (1988); and a preprint (1988).
[17] P. D. I. Fletcher, A. M. Howe, and B. H. Robinson, J. Chem. Soc. Faraday Trans. 1, **83**, 185 (1987).
[18] *Reactions in Compartmentalized Liquids*, edited by W. Knoche and R. Schomacker (Springer, Berlin, 1989).
[19] M. Kahlweit, R. Strey, P. Firman, D. Haase, J. Jen, and R. Schomacker, Langmuir **4**, 499 (1988).
[20] M. Kahlweit, R. Strey, R. Schomacker, and D. Haase, Langmuir **5**, 305 (1989).
[21] M. Kahlweit *et al.*, J. Colloid Interf. Sci. **118**, 436 (1987).
[22] L. Auvray, J. P. Cotton, R. Ober, and C. Taupin, J. Phys. Chem. **88**, 4568 (1984); J. Physique **45**, 913 (1984).
[23] A. de Geyer and J. Tabony, Chem. Phys. Lett. **124**, 357 (1986); **113**, 83 (1985).
[24] D. Guest, L. Auvray, and D. Langevin, J. Physique Lett. **46**, L-1055 (1985).
[25] S. H. Chen and T. L. Lin, in *Thermal Neutron Scattering*, Vol III, edited by D. L. Price and K. Skold (Academic Press, New York, 1987), Chap. 16.
[26] O. Ghosh and C. A. Miller, J. Phys. Chem. **91**, 4528 (1987).
[27] K. Shinoda and H. Kunieda, J. Colloid Interface Sci. **118**, 586 (1987).
[28] W. D. Bancroft, J. Phys. Chem. **17**, 501 (1913).
[29] L. E. Scriven, in *Micellization, Solubilization and Microemulsions*, edited by K. L. Mittal (Plenum, New York, 1977), Vol. 2, p. 877.
[30] E. Y. Sheu, S. H. Chen, and J. S. Huang, J. Phys. Chem. **91**, 3306 (1987).
[31] S. H. Chen, E. Y. Sheu, J. Kalus, and H. Hoffmann, J. Appl. Cryst. **21**, 751 (1988); S. H. Chen and J. Teixeira, Phys. Rev. Lett. **57**, 2583 (1986).
[32] G. S. Grest, I. Webman, S. A. Safran, and L. R. Bug, Phys. Rev. A **33**, 2842 (1986).
[33] P. G. de Gennes, *Scaling Concepts in Polymer Physics* (Cornell University Press, New York, 1979).
[34] P. Debye and A. M. Bueche, J. Appl. Phys. **20**, 518 (1949).
[35] P. Debye, H. R. Anderson, and H. Brumberger, J. Appl. Phys. **28**, 679 (1957).
[36] M. Teubner and R. Strey, J. Chem. Phys. **87**, 3195 (1987).
[37] C. G. Vonk, J. F. Billman, and E. W. Kaler, J. Chem. Phys. **88**, 3970 (1988).
[38] B. W. Ninham, I. S. Barnes, S. T. Hyde, P. J. Derian, and T. Zemb, Europhys. Lett. **4**, 561 (1987); T. Zemb, S. T. Hyde, P. J. Derian, I.S. Barnes, and B. W. Ninham, J. Phys. Chem. **91**, 3814 (1987).
[39] W. Jahn and R. Strey, J. Phys. Chem. **92**, 2294 (1988).
[40] S. Ciccariello and A. Benedetti, J. Appl. Cryst. **18**, 219 (1985).
[41] Z. Y. Wang, M. Konno, and S. Saito, J. Chem. Phys. **90**, 1281 (1989).
[42] See G. Porod, in *Small Angle X-ray Scattering*, edited by O. Glatter and O. Kratky (Academic, New York, 1982), Chap. 2.
[43] W. Jahn and R. Strey, presented at the Second European Colloid and Interface Society Conference, Arcachon, France, September (1988).
[44] B. Widom, (preprint).
[45] G. Gompper and M. Schick, Phys. Rev. Lett. **62**, 1647 (1989).
[46] S. T. Milner, S. A. Safran, D. Andelman, M. E. Cates, and D. Roux, J. Physique (France) **49**, 1065 (1988).